# Potentiostatic Control of Ionic Liquid Surface Film Formation on ZE41 Magnesium Alloy

Jim Efthimiadis,[†] Wayne C. Neil,[†] Andrew Bunter,[†] Patrick C. Howlett,[†] Bruce R. W. Hinton,[†] Douglas R. MacFarlane,[‡] and Maria Forsyth*,[†]

Department of Materials Engineering and School of Chemistry, ARC Centre of Excellence for Electromaterials Science, Monash University, Clayton, Victoria 3800, Australia

**ABSTRACT** The generation of potentially corrosion-resistant films on light metal alloys of magnesium have been investigated. Magnesium alloy, ZE41 [Mg−Zn−Rare Earth (RE)-Zr, nominal composition ~4 wt % Zn, ~1.7 wt % RE (Ce), ~0.6 wt % Zr, remaining balance, Mg], was exposed under potentiostatic control to the ionic liquid trihexyl(tetradecyl)phosphonium diphenylphosphate, denoted $[P_{6,6,6,14}]$[DPP]. During exposure to this IL, a bias potential, shifted from open circuit, was applied to the ZE41 surface. Electrochemical impedance spectroscopy (EIS) and chronoamperometry (CA) were used to monitor the evolution of film formation on the metal surface during exposure. The EIS data indicate that, of the four bias potentials examined, applying a potential of −200 mV versus OCP during the exposure period resulted in surface films of greatest resistance. Both EIS measurements and scanning electron microscopy (SEM) imaging indicate that these surfaces are substantially different to those formed without potential bias. Time of flight-secondary ion mass spectrometry (ToF-SIMS) elemental mapping of the films was utilized to ascertain the distribution of the ionic liquid cationic and anionic species relative to the microstructural surface features of ZE41 and indicated a more uniform distribution compared with the surface following exposure in the absence of a bias potential. Immersion of the treated ZE41 specimens in a chloride contaminated salt solution clearly indicated that the ionic liquid generated surface films offered significant protection against pitting corrosion, although the intermetallics were still insufficiently protected by the IL and hence favored intergranular corrosion processes.

**KEYWORDS:** ionic liquids • trihexyl(tetradecyl)phosphonium • diphenylphosphate • magnesium alloy, ZE41 • impedance spectroscopy • surface film • corrosion

## INTRODUCTION

Recent intensive research efforts into the unique properties and applications of ionic liquids (1, 2) have led to the discovery that certain ionic liquids can form a surface film on reactive metals such as lithium, aluminum, magnesium, and their alloys (3−5). Magnesium and its alloys have become critical in a wide variety of engineering applications in the infrastructure, transportation, automotive, aerospace, and electronic industries (6)—areas in which magnesium's high strength-to-weight ratio can be utilized (7). Despite their desirable properties, the widespread use of magnesium-based alloys is limited because of poor corrosion resistance (8), and much effort is devoted to finding ways to improve the corrosion performance of these materials (9−12).

The specific alloy of interest in this work, ZE41, is a Mg−Zn−RE−Zr-based alloy, and is commonly used in aerospace applications such as aircraft gear-box and generator housings, particularly in military helicopter components because of its lightweight and high temperature mechanical properties (13, 14). In the age-hardened condition, the ZE41 microstructure is composed of an α-Mg matrix, with finely distributed β-phase particles (15), and a eutectic T-phase ($Mg_7Zn_3RE$) distributed at the grain boundaries. A Zr−Zn-rich zone of intermetallic particles, which results from the addition of Zr as a grain refiner, is also present within the central regions of the α-Mg grains (15). These characteristic microstructural features play a significant role in the corrosion of ZE41 alloy, with the $Mg_7Zn_3RE$ (T-phase) having been shown to act cathodically with respect to the α-Mg grains, facilitating corrosion of this latter phase (15). The microstructural and compositional heterogeneity of the ZE41 surface is in large part responsible for its high susceptibility to corrosion (16), and also the difficulty in forming uniform protective films. Ionic liquid treatments to generate corrosion protective films have recently been reported (15, 17), but these also suffer from this difficulty.

Ionic liquids (ILs) are salts that are liquid below 100 °C and are composed of a combination of organic cations and organic/inorganic anions. These materials have a unique and desirable set of physical properties that can be tuned by altering the anion/cation chemistry (18, 19). ILs have proven not only to be of considerable fundamental scientific importance but also to present exciting opportunities as commercial materials for example in electrochemical devices (e.g., batteries, solar cells, fuel cells), tribology, and corrosion protection (2, 4, 18, 20−29). ILs exhibit a range of properties, including in some selected cases, low flammability, low vapor pressure, high thermal stability, and a large electrochemical window (24, 30).

* Corresponding author. Tel: +613 990 54939. Fax: +613 990 20325. E-mail: maria.forsyth@eng.monash.edu.au.
Received for review December 14, 2009 and accepted April 15, 2010
[†] Department of Materials Engineering, ARC Centre of Excellence for Electromaterials Science, Monash University.
[‡] School of Chemistry, ARC Centre of Excellence for Electromaterials Science, Monash University.
DOI: 10.1021/am900889n




ARTICLE

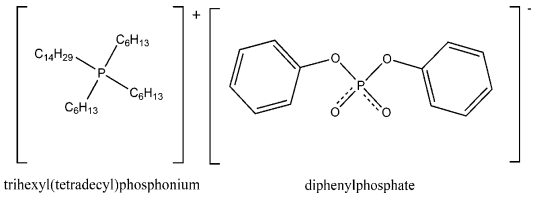


**FIGURE 1. Chemical structures of the ionic liquid, trihexyl(tetradecyl) phosphonium cation, and diphenylphosphate anion, [$P_{6,6,6,14}$][DPP] compound.**

Pertinent to this investigation is the use of ILs in the passivation of reactive metals. Ionic liquids have been shown to improve the corrosion properties of metals and alloys (5, 8, 31), including magnesium and modify the characteristics of the surface film (21). This research into the possible passivation of reactive metals using targeted ILs originated following the discovery of passive film formation on lithium by Howlett and co-workers (5). It has since been shown that a similar surface film can be produced on magnesium and magnesium alloys such as AZ31 (8, 31). In our previous work, the interaction of the IL trihexyl(tetradecyl)phosphonium diphenylphosphate ([$P_{6,6,6,14}$][DPP], Figure 1) with the ZE41 surface has shown that the heterogeneous nature of this surface, because of the complex microstructure described earlier, produced a film on the surface of ZE41 that was not uniform in nature, but in fact was influenced by the surface microstructure of the alloy (17). The IL film deposits were observed to be thickest directly adjacent to the grain boundary phase, with no evidence of interaction on the grain boundary T-phase or the Zr-rich phases within the grain itself. This has led us to investigate methods of activating the metal alloy surface in order to produce a more uniform, and thereby more protective, surface layer.

The method of applying a potential bias to the alloy during exposure to the ionic liquid has been shown here to be a promising method of producing a continuous, protective ionic liquid film on the ZE41 alloy. This work has investigated the formation of the surface film on ZE41 exposed to the ionic liquid [$P_{6,6,6,14}$][DPP] under controlled potentiostatic conditions, through in situ electrochemical monitoring of the surface film evolution with time. The surfaces thus produced were characterized using surface microscopy and ToF-SIMS. Preliminary evaluation of these treated surfaces in chloride contaminated aqueous solutions via immersion studies is also presented.

## EXPERIMENTAL SECTION

**Materials.** Cast magnesium alloy, ZE41 of nominal composition, ~4% Zn, and ~1.7% rare earths (mainly Ce, also Pr, Nd, and La), and ~0.6 wt % Zr (16), in the T5 temper was used as the metallic alloy substrate. Samples 10 mm × 10 mm × 2.5 mm were cut with a Buehler-Isomet diamond saw and polished using 1200 and 4000 grit silicon carbide papers, successively. Following polishing, samples were washed with acetone and distilled water and subsequently dried with nitrogen gas.

**Ionic Liquid Treatment.** The ionic liquid investigated in this work was composed of the diphenylphosphate anion and trihexyl(tetradecyl)phosphonium cation (32), the structures of which are shown in Figure 1. This compound is referred to as [$P_{6,6,6,14}$][DPP]. The synthesis and preparatory route used has been described in detail elsewhere (28). Some key properties of the [$P_{6,6,6,14}$][DPP] ionic liquid are presented below in Table 1 as outlined by Sun et al. in ref 28. The purity of this material was determined and was found to be high (with only negligible levels of acid and $Cl^-$). The presence of water was not determined, as all experiments were performed under ambient conditions.

**Table 1. Properties of the Ionic Liquid Compound, [$P_{6,6,6,14}$][DPP] (28)**

| property | value |
|---|---|
| glass transition temperature (°C) | −72 |
| decomposition temperature (°C) | ~400 |
| conductivity ($^{297}$K) (S $cm^{-1}$) | $1 \times 10^{-5}$ |
| $viscosity_{RT}$ (mPa S) | ~800 |

**Observation of Film Formation via Electrochemical Impedance Spectroscopy (EIS).** A three-electrode pipet cell assembly was used to form and monitor the evolution of the surface film on the alloy. This cell was previously described and preliminary results using this to monitor film evolution on an AZ31 alloy in an ionic liquid has been discussed (33). Approximately 1 mL of [$P_{6,6,6,14}$][DPP] ionic liquid was added to the pipet cell and the ZE41 coupons were exposed to the IL for a 24 h period, during which time electrochemical impedance spectra were acquired at regular intervals. An EG&G PAR VMP2/Z potentiostat was used for all electrochemical measurements, together with the software package ECLab, version 9.53. An electrochemical testing schedule was devised, the test looping 160 times over a 24 h period, measuring the electrochemical impedance spectroscopy over a frequency range 200 kHz to 50 mHz, with 9 sampling points per decade, and 20 mV peak-to-peak AC potential. Biasing experiments were conducted at electrochemical biases of 0, +100, −100, and −200 mV versus the open circuit, the resulting current was also monitored. The potential was gradually stepped to each electrochemical bias, indicated above, as opposed to switching immediately to the stated values, and subsequently held constant at the specified potentials throughout the test. Post-treatment, coupons were washed thoroughly with distilled water and rinsed with ethanol, before being dried with a stream of nitrogen gas. All treatment conditions were repeated in triplicate to ensure the reproducibility of results.

**Surface Characterization by Scanning Electron Microscopy (SEM) and Time of Flight-Secondary Ion Mass Spectrometry (ToF-SIMS).** Scanning electron microscopy (SEM) images were acquired of the biased treated surfaces, the unbiased (OCP) treated surface, and an untreated surface; for comparison. Images were obtained using a JEOL 6490LA SEM and accelerating voltage of 20 keV. Further surface characterization was conducted using a ToF-SIMS IV instrument (ION-TOF GmbH, Germany), equipped with a bismuth primary-ion source to investigate the elemental distribution of IL species across the surface, with etching conducted over a 500 × 500 $\mu$m area and mapping over a 100 $\mu$m × 100 $\mu$m area of the positive and negative ions.

**Evaluation of Corrosion Protection of IL-Generated Films.** The mounted specimens were immersed in a 0.001 M NaCl test solution prepared from analytical grade reagents and distilled water. Magnesium alloys are known to corrode rapidly in most aqueous environments. These rapid rates make a study of the development of the corrosion process difficult. In order to slow the corrosion rate and allow this development to be observed, a mildly aggressive environment 0.001 M NaCl was chosen with a relatively short exposure time of 18 h.

Corrosion product was removed by immersion for 60 s in a solution of 200 g of chromium trioxide ($CrO_3$), 10 g of silver nitrate ($AgNO_3$), 20 g of barium nitrate ($Ba(NO_3)_2$), with distilled

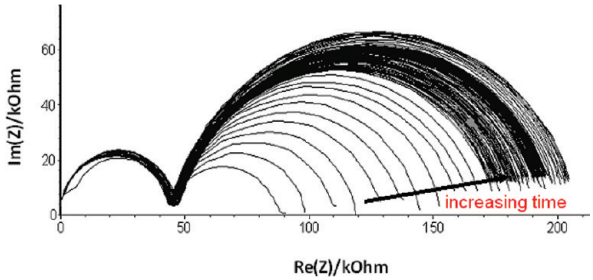


FIGURE 2. Typical Nyquist impedance spectra obtained during treatment at −200 mV versus OCP.

water to make 1000 mL, in accordance with ASTM Standard G1−90, Designation C5.2. Specimens were then analyzed using SEM microscopy as discussed above.

## RESULTS AND DISCUSSION

**Electrochemical Impedance Monitoring of Surface Film Evolution.** Figure 2 shows the evolution of the impedance spectra, obtained as a function of time-over a 24 h period for a ZE41 coupon biased to −200 mV versus OCP. It is evident from this figure that there is a clear trend in the impedance, with both $Z$ and $Z'$ (real and imaginary parts of impedance, respectively), increasing with treatment time. Two semicircles are observed in the spectra, indicative of at least two processes occurring. This behavior persists throughout the duration of the experiment.

The evolution of the impedance spectra with time ($t = 0$, 12, and 24 h) for four different potentials, −200, −100, and +100 mV and OCP, are shown in Figure 3. The influence of the bias potential on the impedance response is clearly revealed. At the initial stage of treatment (Figure 3A, $t = 0$); there is no significant difference in impedance between any of the applied potentials, although −200 mV bias has a slightly higher real axis touchdown point of 29 kOhm cm$^2$ relative to the other measured impedance real axis intercept (~20 kOhm cm$^2$, at time $t = 0$ h). After 12 h (Figure 3B), clear trends begin to emerge; multiple semicircles are observed, increasing in impedance as the bias changes from +100 mV, 0 mV (i.e., at OCP), −100 mV, and −200 mV. The positive applied potential results in a lower real axis intercept (i.e., resistance) even compared with the treatments performed at OCP. It also seems that the larger the magnitude of the negative applied potential, the larger the impedance. This effect is more exaggerated after 24 h of treatment (Figure 3C). The magnitude of the resistance increase appeared to increase proportionally with the magnitude of the bias applied. This can be further quantified through equivalent circuit modeling, as discussed below in the case of the surface biased at −200 mV versus OCP.

The electrochemical impedance spectroscopy data obtained were modeled using the computer package ECLab, version 9.53. This package was used to fit an equivalent resistive-capacitive circuit to the data. The best fitting (and simplest) model that gave good agreement with the data was assigned the processes shown in Figure 4A. An example fit is shown in Figure 4B. The evolution of the circuit parameters was analyzed as follows. The resistance of the second

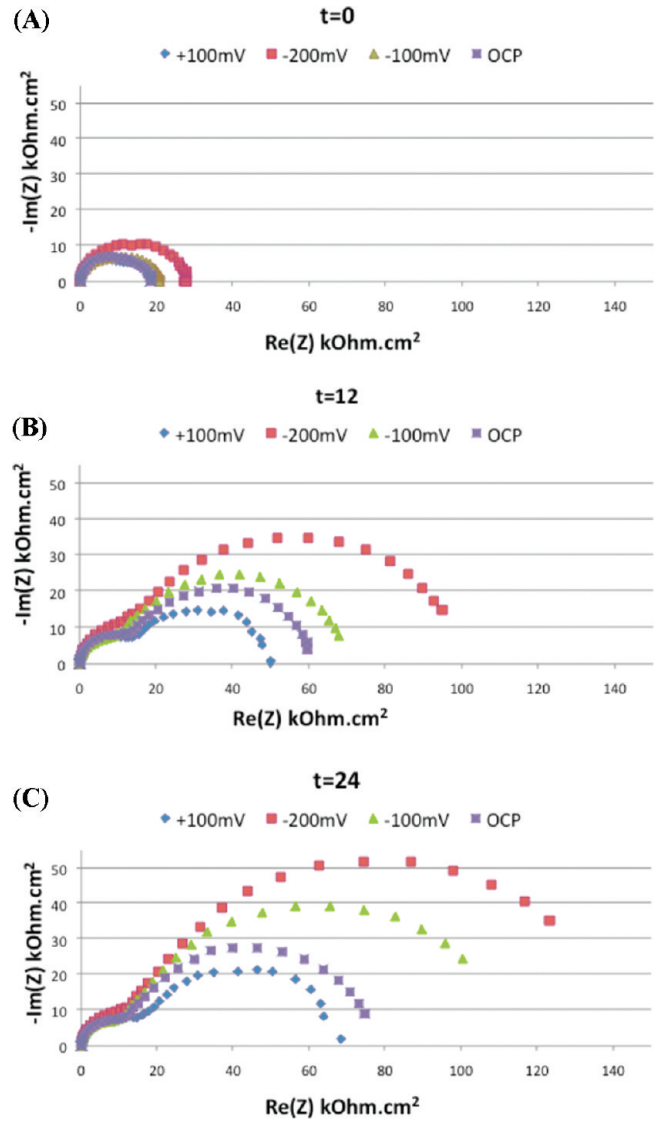


FIGURE 3. Effect of biasing over time. Each plot shows curves for experiments run at open circuit potential (OCP), +100 mV versus OCP, −100 mV versus OCP, and −200 mV versus OCP. (A) initial frequency response, (B) the response after 12 h, and (C) the response after 24 h.

RC element ($R_3$, Figure 4C) was found to increase initially, and then dip and eventually plateau out, whereas the other circuit parameters remained constant. The evolution of the resistive parameter $R_3$ can be attributed to the evolution and growth of the film over time. On the basis of this analysis, it is expected that the most protective surface would be obtained after a treatment time of 4−5 h, close to the maximum value of $R_3$. Further optimization of these surface films and an investigation of their corrosion resistance is currently underway.

**Interfacial Processes in the IL.** Chronoamperometry data was also acquired during these experiments (Figure 5). Part of the current response might be viewed as being analogous to double layer formation; in one model, these surfaces can be viewed as modified oxide films where the native oxide film has been penetrated by the IL ions. Spectroscopic evidence suggests that in the case of [$P_{6,6,6,14}$][DPP] this involves an interaction with the DPP

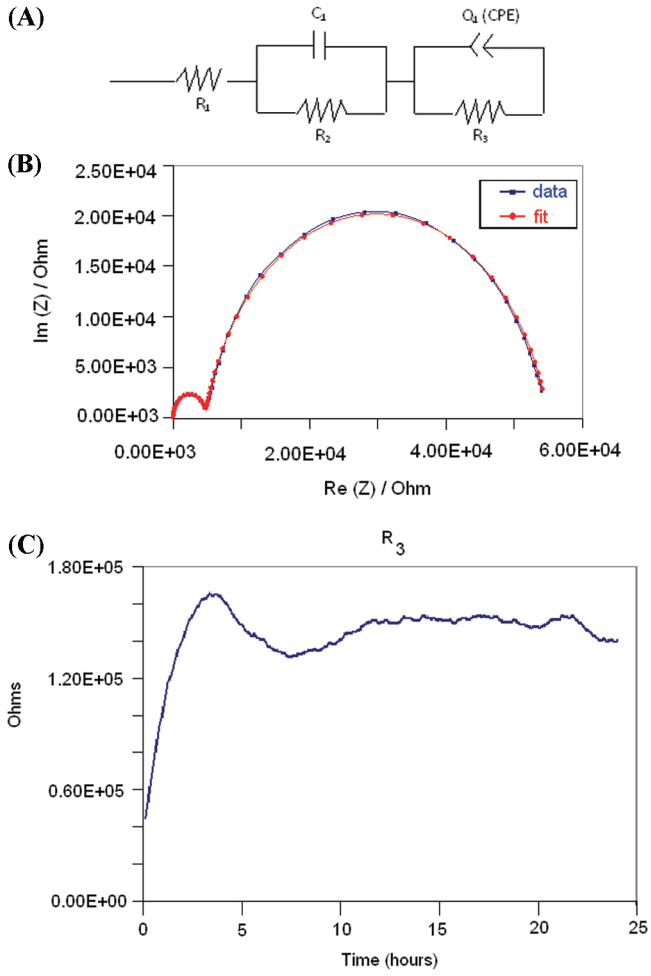


**FIGURE 4. (A) Fitted EIS equivalent circuit, average CPE *a* parameter value of 0.87. (B) Example fit of equivalent circuit given in A. (C) Film resistance ($R_3$) for duration of testing.**

anion, which is apparently dependent upon the presence of OH groups on the surface of the oxide (17). The adsorption of the anion subsequently binds the cation electrostatically.

**Scheme 1. Chemical Reactions Proposed to Occur at the Surface**

(1) $2H_2O + 2e^- \rightleftharpoons H_2 + 2OH^-$

(2) $O_2 + 4e^- + 2H_2O \rightleftharpoons 4OH^-$

(3) $Mg \rightleftharpoons Mg^{2+} + 2e^-$

(4) $Mg + 2OH^- \rightleftharpoons Mg(OH)_2 + 2e^-$

(5) $M + xH_2O \rightleftharpoons M(OH)_x + x/2\ H_2$ (where M is Ce, Zr, Zn or Mg)

(6) $Mg^{2+} + 2DPP^- \rightleftharpoons Mg(DPP)_2$

(7) $Mg^{2+} + DPP^- + OH^- \rightleftharpoons Mg(DPP)(OH)$

It may be possible that this process of relatively slow charging of the surface could manifest as a charging current in the measurements shown here. However, it is expected that currents associated with such processes would be very small.

On the other hand, under the applied bias, the current response is most likely dominated by some redox process. As apparent from Figure 5, a positive bias results in an oxidation process and a negative bias results in a reduction process. Considering the available reactive species, the following reactions (Scheme 1) can be proposed to be occurring at the surface regardless of any applied bias potential.

We have also proposed the electrochemical reduction of the DPP anion itself, involving cleavage of one of the phenyl groups as a mechanism of film formation (17). This process may occur at all of the applied biases.

A further complicating factor in understanding the chemical process occurring in these experiments comes from the expected changes in the stoichiometry of the species at the metal interface upon application of a bias potential; a negative bias will lead to a dominance of the $[P_{6,6,6,14}]^+$

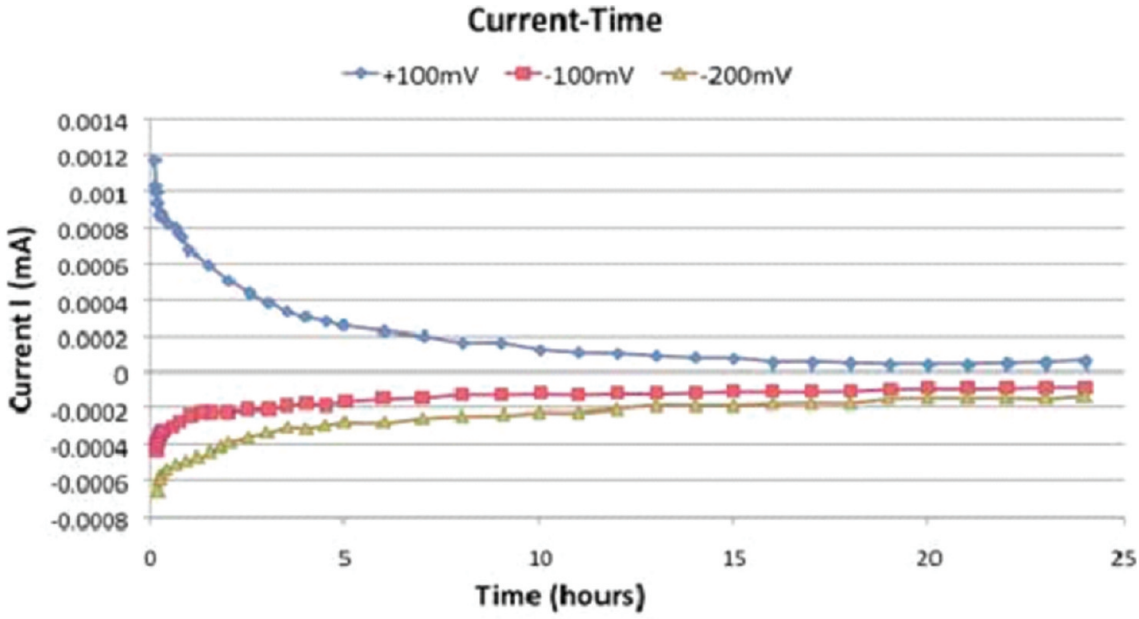


**FIGURE 5. Current (mA) versus time (hours) for each of +100, −100, and −200 mV versus OCP.**

cation, which is thought to be weakly interacting with the surface, as well an increase in the rate of the water reduction reaction. Alternatively, for a positive bias, there will be a dominance of the $[DPP]^-$ anion, thought to be strongly interacting, and an increase in the rate of the Mg dissolution reaction. This likely shift in stoichiometry at the interface may alter the composition and morphology of the deposited film.

It is apparent from Figure 5 that the amount of charge (i.e., the area under the curve) during the +100 mV biased treatment, was greater than either of the negative potential treatments. This is indicative of a greater reaction occurring at the surface, and possibly the formation of a thicker film (if the products are all insoluble or of similar solubility). However, the results seen from the impedance spectroscopy experiments, would suggest that this film is highly defective and hence provides a lower resistance as compared to those surfaces produced using a negative bias potential. Such behavior has also been observed previously for AZ31 exposed to phosphonium-based IL for extended periods of time (31).

**Surface Characterization Following IL Exposure.** SEM images of an untreated, polished, ZE41 magnesium alloy surface, a surface after a 24 h IL treatment at OCP, and a surface after a −200 mV bias treatment are shown in Figure 6. The difference in surface detail appearance between the three surfaces of the same substrate−metal is immediately obvious. Both treated samples appear to be different from the as-received, untreated surface, Figure 6A. It has previously been noted (17) that the resultant surface from exposure of a ZE41 alloy to the diphenyl phosphate IL of interest in this work is highly heterogeneous with a build up of reaction product next to the grain boundary and no apparent interaction on the intermetallic surfaces. This was explained in terms of the higher reactivity of the Mg alloy next to the grain boundary and the lack of interaction between the ionic liquid and the phases present on the grain boundaries. The application of a negative bias seems to remove this preference for film deposition, leading to an apparently more homogeneous surface.

This homogeneity is further evidenced by the Time of Flight Secondary Ion Mass Spectroscopy (ToF-SIMS) as seen in Figure 7. ToF-SIMS is a surface sensitive analytical technique that facilitates the probing of the uppermost (or outermost) layers of the test specimen for the elemental mapping and identification of elemental states of the organic cation and anion. Its penetration depth is on the order of few atomic monolayers. Although not a quantitative technique, ToF-SIMS provides an insight into the chemical state of the elements and molecules present and their distribution at the metal surface.

The data clearly indicates the presence of fragments from both the IL anion (DPP) and cation ($P_{6,6,6,14}$) with the presence of $PO_2$, $PO_3$, and CH, $C_2$, $C_2H$, and $C_2H_5$, fragments as well alkyl moieties associated with the fragmentation of the cation. This is clear evidence for the presence of an IL-based surface film. Figure 7 contrasts the ToF-SIMS negative ion maps in the case of the ZE41 sample at 24 h OCP (i.e., without a bias potential applied) and the −200 mV bias sample, in order to observe differences in the film morphology. These maps reveal the presence of $OH^-$ (associated with the $Mg(OH)_2$), $C_6H_5O$, and $PO_3$, all concentrated primarily at the grain boundary in the absence of a bias potential (Figure 7 A), hence providing further evidence that the ionic liquid preferentially reacts near the grain boundary regions (17). The negative ion map of the biased sample reveals a more uniformly distributed ionic liquid film with similar chemical features. Furthermore, the total ion count is greater for the biased sample, perhaps indicative of a thicker, more homogeneous film.

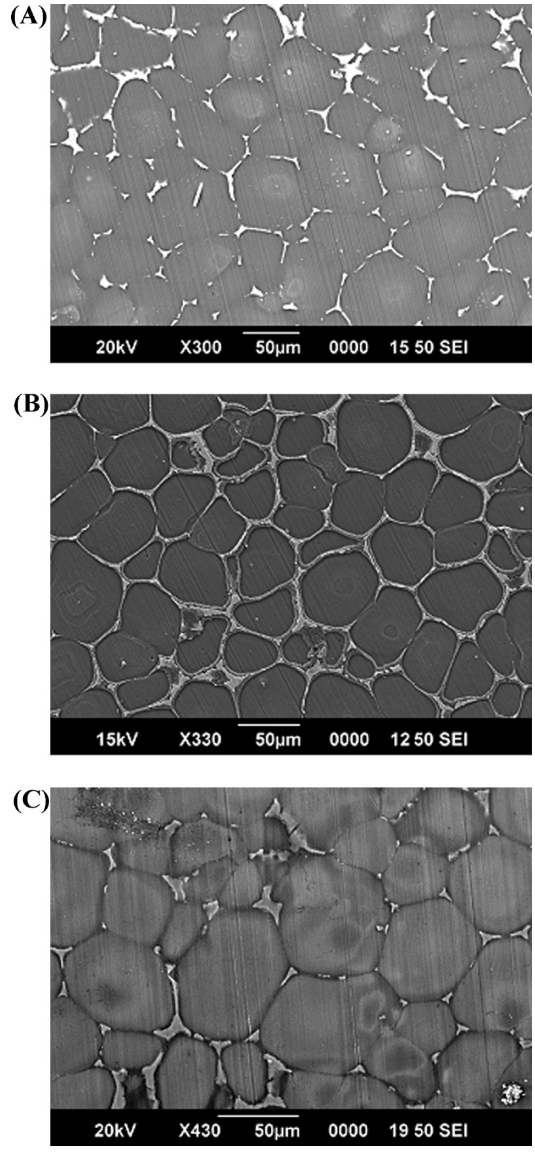


**FIGURE 6. (A) SEM image of ZE41 surface as-polished; (B) SEM image of a ZE41 surface after 24 h treatment at OCP. (C) SEM image of a ZE41 surface after 24 h treatment biased to −200 mV versus OCP.**

The composition and mechanism of deposition of the IL surface film on a ZE41 alloy under simple immersion of the alloy in the $[P_{6,6,6,14}][DPP]$ ionic liquid has previously been discussed (17). Furthermore, it has previously been shown, using solid-state NMR spectroscopy, that IL−surface interactions on an inorganic oxide surface (as would be present on any reactive metal) are dependent on the presence of

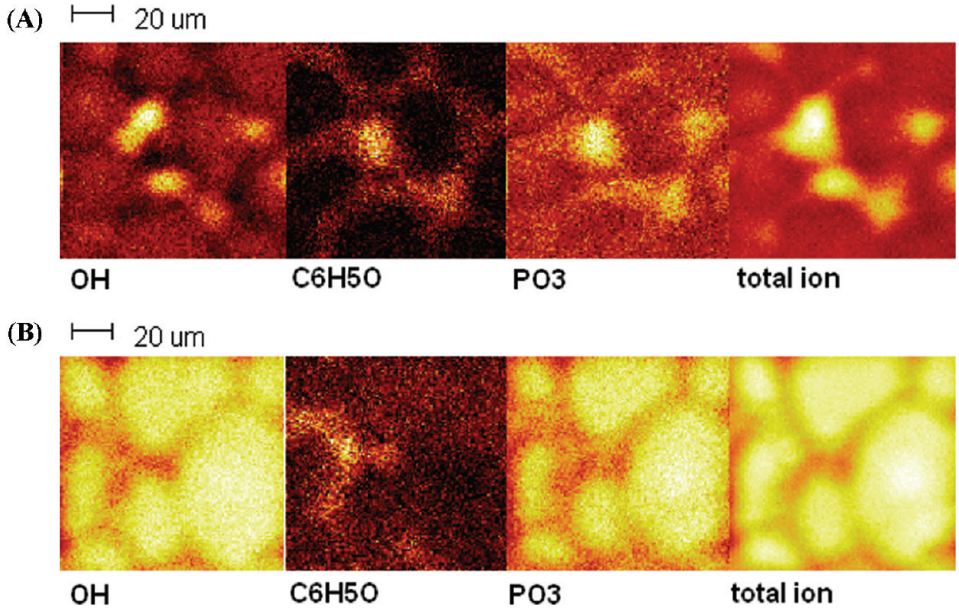


**FIGURE 7. ToF-SIMS mapping of selected elements and molecules for the ZE41 magnesium alloy at (A) 24 h OCP and (B) −200 mV biasing.**

hydroxide surface groups (20). As proposed earlier, the negative bias is likely to result in the formation of $OH^-$ (reactions 1 and 2 in Scheme 1) uniformly across the metal surface. If the mechanism of film formation involves the interaction of the $[DPP]^-$ anion with the $OH^-$ surface, the negative biasing would promote a uniform film. Furthermore, if the reduction of the $[DPP]^-$ is integral to the resultant surface film then this too would occur more uniformly on the biased surface and hence result in a uniform surface film.

**Corrosion Protection of IL-Generated Films.** The SEM images presented in Figure 8 indicate that the exposure of the ZE41 alloy to IL both under OCP conditions and during a −200 mV biasing treatment have a significant affect on the corrosion processes in a $Cl^-$ contaminated aqueous solution. These tests were purposefully conducted at low $Cl^-$ concentrations to discriminate any differences in this preliminary testing, bearing in mind that the IL-generated films are not optimized for corrosion protection at this stage. It was therefore very promising to observe that the intense pitting generated by the $Cl^-$ solution on the untreated specimen was significantly suppressed upon exposure of the ZE41 alloy to the DPP IL under both OCP and bias conditions. Clearly, the film generated in the IL (as was observed via ToF-SIMS experiments) was more resistant to $Cl^-$ ions as compared with the native oxide/hydroxide film on the untreated specimen. What is interesting to note here is that the biasing treatment further reduces the corrosion within the α-Mg grains; however, it does not appear to suppress the grain boundary corrosion processes. This is in contrast to the surface films generated in the absence of a bias potential, which seemed to have a greater effect on the corrosion processes at the grain boundary, probably due to the favored deposition of an IL-based film adjacent to the grain boundaries, as shown by ToF-SIMS data. It appears, therefore, that the $Mg_7Zn_3RE$ (T-phase) does not react favorably with the $[DPP]^-$ IL used in this work even under cathodic bias conditions. Future work will need to address alternative IL chemistry that will enable a more uniform surface film across such a heterogeneous alloy surface; this may for example involve mixtures of ILs or consecutive treatments.

## CONCLUSIONS

Electrochemical impedance spectroscopy experiments have been used to monitor surface film evolution on a ZE41 alloy exposed to a $[P_{6,6,6,14}][DPP]$ ionic liquid under zero bias, negative bias, and positive bias (compared to open circuit potential OCP) conditions. It was found that applying a potential bias of −200 mV versus OCP during a 24 h period produces surface films of significantly higher resistance than can be achieved without bias. The magnitude of the resistance increase appeared to increase proportionally with the magnitude of the bias applied. In addition, applying positive potentials produced a film of reduced resistance compared to open circuit conditions. EIS also gave an insight into the nature of the surface film formation during treatment, with modeling of the surface behavior indicating that the resistance of the film increased with time, relating to the development of a thicker surface film. SEM indicated that the surface film on ionic liquid treated ZE41 coupons was markedly different to an untreated surface, and furthermore the −200 mV biased alloy had a significantly more uniform film deposition compared to the film produced after 24 h at OCP. The ToF-SIMS images also indicated the deposition of a homogeneous film under bias conditions. Hence, the morphology of the surface can be altered by biasing the treated surface to potentials away from OCP during exposure to the IL. The surfaces generated under both OCP and −200 mV bias conditions were evaluated for corrosion performance using immersion testing in 0.001 M $Cl^-$ aqueous solutions and found to offer significant protection against pitting corrosion, particularly within the α-Mg grain itself. Further understanding of the effects of this bias treatment

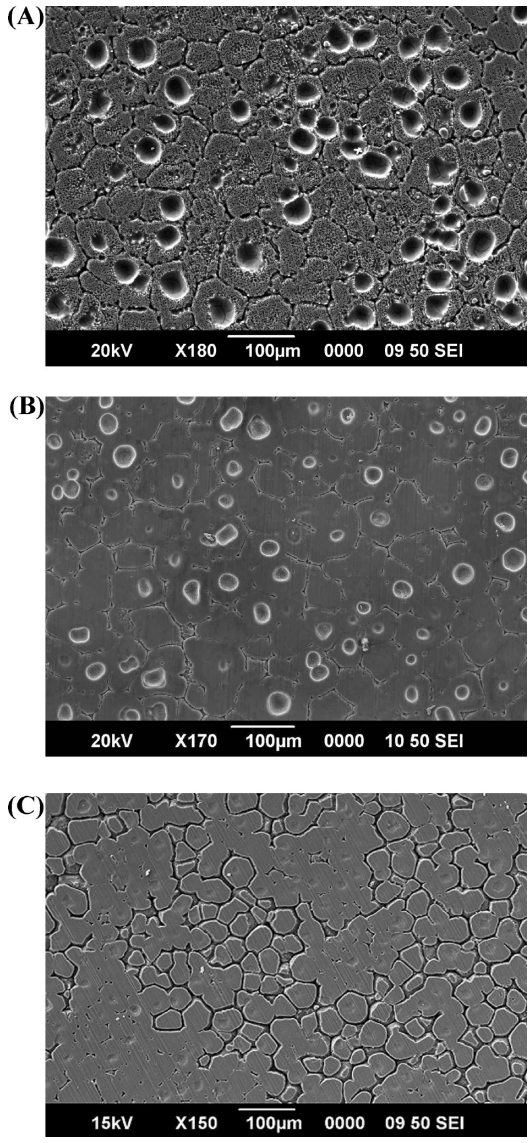


**FIGURE 8. SEM images of ZE41 alloys surfaces post 18 h immersion in 0.001 M NaCl solutions: (A) untreated control, (B) DPP treatment at OCP after 24 h, (C) DPP treatments at −200 mV bias for 24 h. The changes in corrosion morphology are clearly evident upon IL immersion with pitting within the grain suppressed in both IL-treated cases and favoring of grain boundary corrosion post-biasing treatment.**

and elucidation of the mechanism of film formation could lead to improved surface films and more effective corrosion resistance.

**Acknowledgment.** The authors gratefully acknowledge the ARC for financial support, through Grant DP0986205, the ARC Centre of Excellence for Electromaterials Science, and D.R.M.'s Federation Fellowship. We also appreciate the mechanical and electronics support of the Mechanical workshop of the School of Physics at Monash University, Clayton, Australia. Robert Jones of the Centre for Materials and Surface Science, Department of Physics, Latrobe University, is thanked for ToF-SIMS acquisition.

## REFERENCES AND NOTES

(1) Anthony, J. L.; Brennecke, J. F.; Holbrey, J. D.; Maginn, E. J.; Mantz, R. A.; Rogers, R. D.; Trulove, P. C.; Visser, A. E.; Welton, T. In *Ionic Liquids in Synthesis*; Wasserscheid, P., Welton, T., Eds.; Wiley-VCH Verlag GmbH & Co. KGaA: Weinheim, Germany, 2002; Vol. 1, p 41.
(2) MacFarlane, D. R.; Forsyth, M.; Howlett, P. C.; Pringle, J. M.; Sun, J.; Annat, G.; Neil, W.; Izgorodina, E. I. *Acc. Chem. Res.* **2007**, *40*, 1165–1173.
(3) NuLi, Y.; Yang, J.; Wu, R. *Electrochem. Commun.* **2005**, *7*, 1105–1110.
(4) Bermudez, M. -D.; Jiménez, A. -E.; Martínez-Nicolás, G. *Appl. Surf. Sci.* **2007**, *253*, 7295–7302.
(5) Howlett, P. C.; Brack, N.; Hollenkamp, A. F.; Forsyth, M.; MacFarlane, D. R. *J. Electrochem. Soc.* **2006**, *153*, A595–A606.
(6) Aghion, E.; Bronfin, B. *Mater. Sci. Forum* **2000**, *350−351*, 19–30.
(7) Song, G. L.; Atrens, A. *Adv. Eng. Mater.* **1999**, *1*, 11–33.
(8) Birbilis, N.; Howlett, P. C.; MacFarlane, D. R.; Forsyth, M. *Surf. Coat. Technol.* **2007**, *201*, 4496–4504.
(9) Kouisni, L.; Azzi, M.; Zertoubi, M.; Dalard, F.; Maximovitch, S. *Surf. Coat. Technol.* **2004**, *185*, 58.
(10) Baudrand, D. *Plat. Surf. Finish.* **2005**, *92*, 30–34.
(11) Gray, J. E.; Luan, B. *J. Alloys Compd.* **2002**, *336*, 88–113.
(12) Hu, J.; Shaokang, G.; Zhang, C.; Ren, C.; Wen, C.; Zeng, Z.; Peng, L. *Surf. Coat. Technol.* **2009**, *203*, 2017–2020.
(13) Howlett, P. C.; Neil, W. C.; Khoo, T.; Sun, J.; Forsyth, M.; MacFarlane, D. R. *Isr. J. Chem.* **2008**, *48*, 313–318.
(14) McAdam, G.; Talevski, J.; Trueman, A. R.; Danek, S.; Hinton, B. R. W. *Corros. and Mater.* **2005**, *30*, 13–20.
(15) Neil, W. C.; Forsyth, M.; Howlett, P. C.; Hutchinson, C. R.; Hinton, B. R. W. *Corros. Sci.* **2009**, *51*, 389–394.
(16) Carboneras, M.; Lopez, M. D.; Rodrigo, P.; Campo, M.; Torres, B.; Otero, E.; Rams, J. *Corros. Sci.* **2010**, *52*, 761–768.
(17) Forsyth, M.; Neil, W. C.; Howlett, P. C.; MacFarlane, D. R.; Hinton, B. R. W.; Rocher, N.; Kemp, T. F.; Smith, M. E. *ACS Appl. Mater. Interfaces* **2009**, *1*, 1045–1052.
(18) Wei, D.; Ivaska, A. *Anal. Chim. Acta* **2008**, *607*, 126–135.
(19) Martin, J. D. In *Ionic Liquids: Industrial Applications for Green Chemistry*; Rogers, R. D., Seddon, K. R., Eds.; ACS Symposium Series; American Chemical Society: Washington, D.C., 2002; Vol. 818, pp 413−442.
(20) Forsyth, M.; Kemp, T. F.; Howlett, P. C.; Sun, J.; Smith, M. E. *J. Phys. Chem. Lett.* **2008**, *112*, 13801–13804.
(21) Caporali, S.; Ghezzi, F.; Giorgetti, A.; Lavacchi, A.; Tolstogouzov, A.; Bardi, U. *Adv. Eng. Mater.* **2007**, *9*, 185–190.
(22) Liu, N.; Wu, D.; Wu, H.; Luo, F.; Chen, J. *Solid State Ionics* **2008**, *10*, 1049–1055.
(23) Simka, W.; Puszczyk, D.; Nawrat, G. *Electrochim. Acta* **2009**, *54*, 5307–5319.
(24) Seddon, K. R. *J. Chem. Technol. Biotechnol.* **1997**, *68*, 351–356.
(25) Borgel, V.; Markevich, E.; Aurbach, D.; Semrau, G.; Schmidt, M. *J. Power Sources* **2009**, *189*, 331–336.
(26) Vasudeva Rao, P. R.; Vankatesan, K. A.; Srinivasan, T. G. *Prog. Nucl. Energy* **2008**, *50*, 449–455.
(27) Predel, T; Pohrer, B; Schlücker, E. *Chem. Eng. Technol.* **2009**, *33*, 132–136.
(28) Sun, J.; Howlett, P. C.; MacFarlane, D. R.; Forsyth, M. *Electrochim. Acta* **2008**, *54*, 254–260.
(29) Howlett, P. C.; Zhang, S.; MacFarlane, D. R.; Forsyth, M. *Aust. J. Chem.* **2007**, *60*, 43–46.
(30) El Abedin, S. Z.; Endres, F. *Acc. Chem. Res.* **2007**, *40*, 1106–1113.
(31) Forsyth, M.; Howlett, P. C.; Tan, S. K.; MacFarlane, D. R.; Birbilis, N. *Electrochem Solid-State Lett.* **2006**, *9*, B52-B55.
(32) Chang, T.; Robertson, A.; Kamenetzky, E.; Rivera, C.; Du, L.; Harris, D.; Piquette, M.; Nucciarone, D.; Crutchfield, C. *Ionic Liquids IV: Not Just Solvents Anymore*; Brennecke, J. F., Rogers, R. D., Seddon, K. R., Eds.; ACS Symposium Series; American Chemical Society: Washington, D.C., 2007; Vol. 975, pp 47−68.
(33) Howlett, P. C.; Khoo, T.; Mooketsi, G.; Efthimiadis, J.; MacFarlane, D. R.; Forsyth, M. *Electrochim. Acta* **2010**, *55*, 2377–2383.

AM900889N